

ORBIT DETERMINATION OF ROSETTA AROUND COMET 67P/CHURYUMOV-GERASIMENKO

**Bernard Godard⁽¹⁾, Frank Budnik⁽²⁾, Pablo Muñoz⁽³⁾, Trevor Morley⁽¹⁾, and Vishnu
Janarthanan⁽⁴⁾**

⁽¹⁾*Telespazio VEGA Deutschland GmbH, located at ESOC**

⁽²⁾*ESA/ESOC**

⁽³⁾*GMV, located at ESOC**

⁽⁴⁾*Terma GmbH, located at ESOC**

**Robert-Bosch-Str. 5, 64293 Darmstadt, Germany, +49 6151 900,*

< firstname > . < lastname > @esa.int (remove letter accents)

Abstract: *When Rosetta arrived at comet 67P/Churyumov-Gerasimenko in early August 2014, not much was known about the comet. The orbit of the comet had been determined from years of tracking from ground observatories and a few months of optical tracking by Rosetta during approach. Ground and space-based images had also been used to construct light curves to infer the comet rotation period. But the comet mass, spin axis orientation and shape were still to be determined. The lander Philae was scheduled to land in about three months at a date chosen as a compromise between the time required to acquire sufficient knowledge about the comet and the risk of rising comet activity worsening the navigation accuracy. During these three months, the comet had to be characterised for navigation purposes. In particular, the comet orbit, attitude, centre of mass and gravity field had to be determined. This paper describes the Rosetta orbit determination process including the comet parameters determination, the dynamic and observation models, the filter configuration, the comet frame definition and will discuss the achieved navigation accuracy.*

Keywords: *Rosetta orbit determination, small body relative optical navigation, gravity field determination, comet attitude and orbit determination, 67P/Churyumov-Gerasimenko*

1. Introduction

Launched in March 2004, Rosetta is an ESA mission to study comet 67P/Churyumov-Gerasimenko. 10 years later, in 2014, after 3 Earth swing-bys [1], one Mars swing-by [2], two asteroid flybys [3], [4] and a long deep space hibernation period, Rosetta reached its target. The navigation during approach is described in [5]. Rosetta carried a small lander, Philae, that was deployed on the surface on November 12, 2014. This paper is concerned with the navigation from arrival at comet in August 2014 to the week before lander delivery. During this period, the navigation accuracy had to be improved to allow a sufficiently accurate landing of Philae. The navigation for the landing phase itself is described in [6].

This section briefly describes the Rosetta spacecraft, navigation problem and mission phases. Sections 2., 3. and 4. respectively describe the dynamic models, observation models and estimation filter of the orbit determination program. Section 5. describes the operational setup and navigation results.

1.1. Rosetta Spacecraft

Rosetta is a 3-axis stabilised spacecraft. Roughly speaking the spacecraft frame is defined as follows:

- The +Z face houses the instruments including the scientific and navigation cameras and is usually pointed at the comet.
- The thrusters that are used for orbit control are mounted on the -Z face with the launcher interface.
- The steerable High Gain Antenna (HGA) is on the +X face and thus the Earth direction is usually in the positive X half-space.
- The lander and star-trackers are on the -X face which normally stays cold.
- The Y axis is the solar panels articulation axis and is nominally orthogonal to the Sun direction.

In normal mode, the spacecraft attitude is determined using a gyro-stellar estimator and is controlled with 4 reaction wheels. To manage angular momentum, desaturation manoeuvres must be performed regularly. During the mission phase of interests here, there were about two of those per Earth day. The reaction control system is balanced so that there is only a stochastic residual velocity change (ΔV) for each desaturation manoeuvre.

Rosetta is equipped with 2 navigation cameras (NAVCAM) with a field of view of 5 degrees and a pixel angular size of 5 millidegrees. Additionally the Narrow Angle Camera (NAC) and Wide Angle Camera (WAC) of the OSIRIS scientific instrument are sometimes used for navigation purposes. The NAC field of view is 2.2 degrees for a pixel size of 1.1 millidegree. The WAC field of view is larger than 10 degrees and its pixel size is 5.8 millidegrees [7].

1.2. Overview of navigation problem

During cruise, Rosetta had been navigated using 2-way Doppler and range tracking in X-band, sometimes augmented by Delta-DOR. For the purpose of relative navigation during comet approach, inertial directions from Rosetta to the comet as seen by the spacecraft navigation or scientific cameras had additionally been input to the orbit determination system which was then also solving for the comet orbital state. During the proximity phase, because the comet was now well resolved in the camera and because it was necessary also to determine the comet orientation, these inertial directions to comet measurements had to be replaced by observations of recognisable surface features, so-called landmarks. From that point onwards, Rosetta orbit determination has been solving for a state vector which includes the comet and spacecraft orbital states and the comet attitude state. The observations available for navigation are summarised in Fig. 1. The ground-based optical astrometric comet observations are nominally not individually processed in Rosetta Orbit Determination. Instead they are used to compute an independent long arc orbit solution which is then used to constrain a priori the comet orbital state in Rosetta Orbit Determination [5].

We are mainly interested in the relative state between the spacecraft and the comet. The landmark observations are the most direct measurement of this relative state. Similarly, we are interested in the relative dynamics which is summarised in Fig. 2. The main forces acting on the spacecraft are

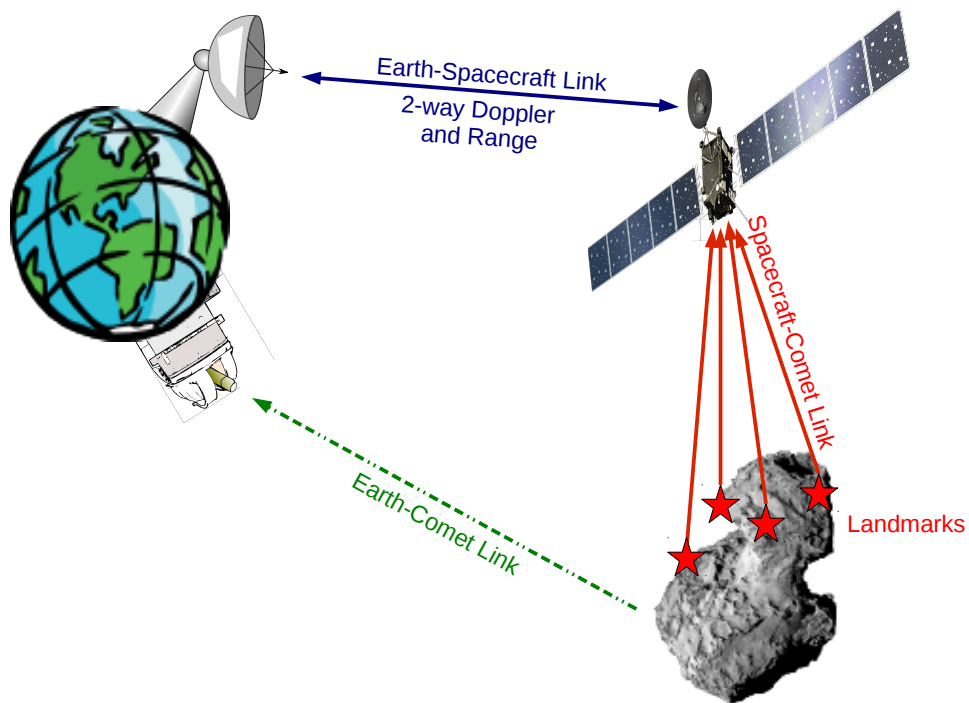


Figure 1. Observables

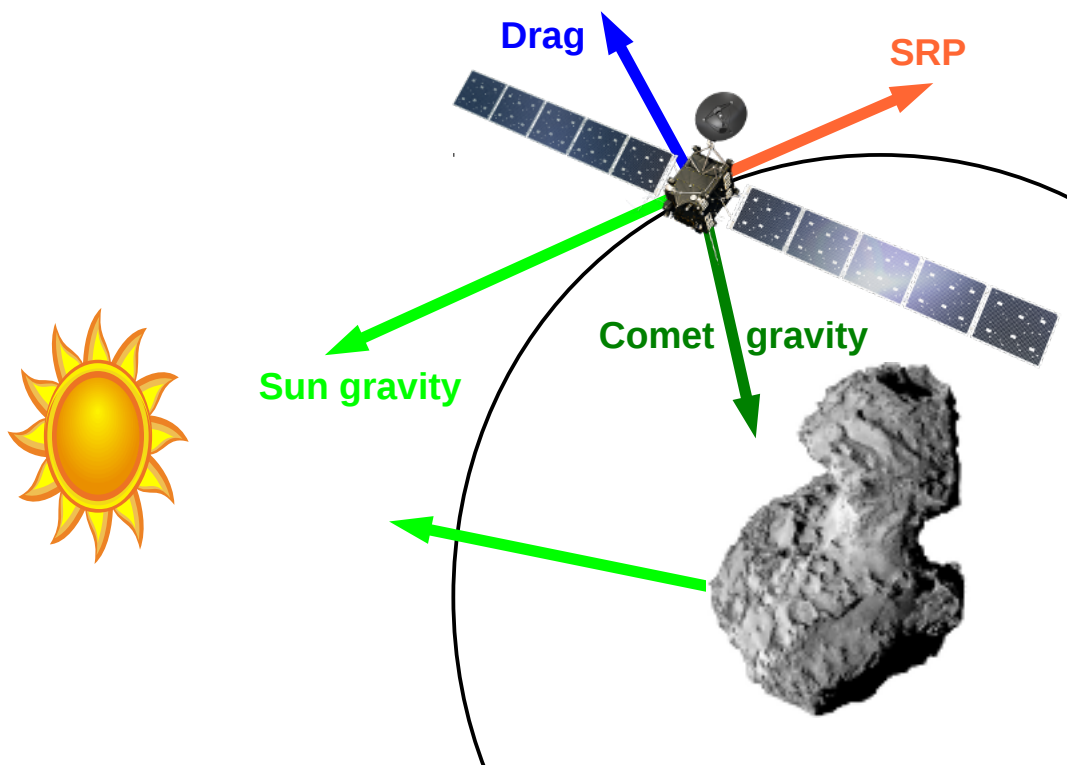


Figure 2. Dynamics

the comet gravity which is almost radial, the Sun third-body gravity, the Solar Radiation Pressure (SRP) which points away from the Sun and the drag force due to the coma. Because the velocities of the gas in the coma (hundreds of meters per second) is much higher than the spacecraft velocity (sub meter per second), the drag acceleration is mainly in the radial direction.

1.3. Mission phases

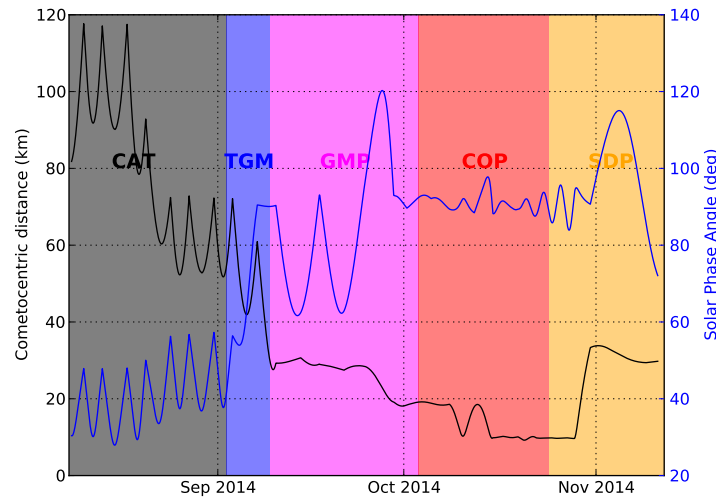


Figure 3. Evolution of cometocentric distance and solar phase angle

The mission phases with which this paper is concerned are listed in Tab. 1 and the evolution of the relative trajectory during that period is represented in Fig. 3, Fig. 4 and Fig. 5. In Fig. 5, the X axis is the Sun direction, and the Z axis is the projection of the comet spin vector on the plane orthogonal to X.

Table 1. Mission phases

Acronym	Phase name	Start Date
CAT	Close Approach Trajectory	2014/08/01
TGM	Transition to Global Mapping phase	2014/09/02
GMP	Global Mapping Phase	2014/09/09
COP	Close Observation Phase	2014/10/06
SDP	Science surface package Delivery Phase	2014/10/24

From August 1, 2014 to November 11, 2014, the heliocentric distance decreased from 3.6 to 3.0 AU, the geocentric distance increased from 2.7 to 3.4 AU and the angle between the Sun and Earth direction was less than 20 degrees.

An important trajectory design parameter during this period was the solar phase angle: the angle between the comet to spacecraft vector and the comet to sun vector. For low phase angles, the camera images of the comet contain little shadows while for very large phase angles (close to 180 degrees) images show a very dark and barely visible comet which is not desirable for navigation

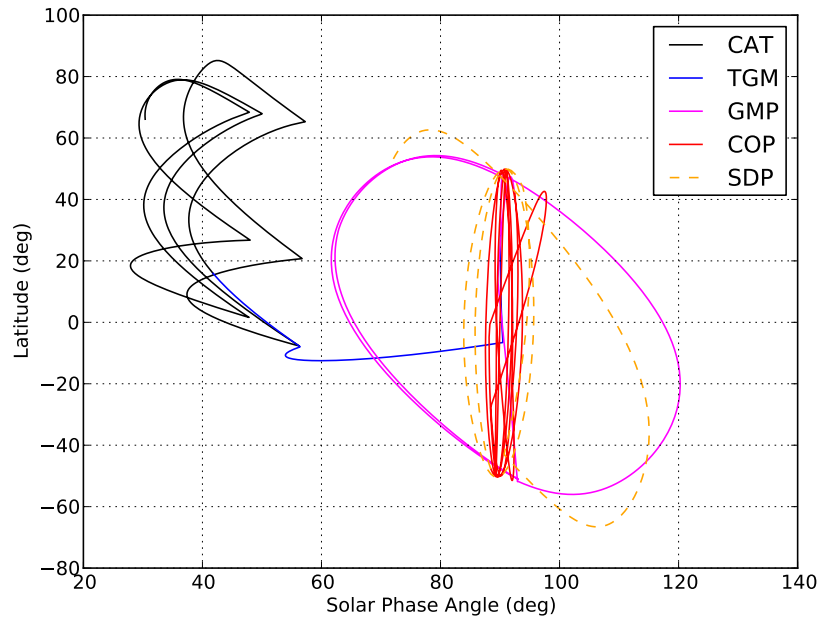


Figure 4. Cometocentric latitude versus solar phase angle

purposes. In the terminator plane (region where the solar phase angle is 90 degrees), the large solar panels are oriented in a direction orthogonal to the comet direction and thus the cross-sectional area of the spacecraft in the direction of the comet is minimised, reducing significantly the acceleration of the spacecraft due to drag and the associated navigational errors. Moreover, it is believed that the coma is more active on the day-side of the comet where the solar phase angle is below 90 degrees. Hence, the terminator is the place to be for accurate navigation at close distance.

In the CAT phase, the spacecraft was flying hyperbolic arcs in front of the comet as seen from the Sun at low phase angles, providing a good view of the comet. The comet distance was initially about 100 km and was later reduced to about 60 km. During this phase, the first landmark observations were processed, the mass and rotational state of the comet were roughly determined. The TGM phase was a short transfer trajectory. In GMP, the spacecraft was flying bound orbits at 30 km radius with a larger phase angle. The goal there was to map the visible (the southern latitude regions were dark and would remain so for many months) part of the comet, that is to cover it with landmarks. In COP, the spacecraft was flying terminator orbits first at 20 kilometre radius then at 10. During that phase, the knowledge on the comet centre of mass and gravity field was improved significantly. In the beginning of the SDP phase, the spacecraft was brought back to a 30 kilometre orbit to prepare for lander delivery.

1.4. Space and time references

Rosetta orbit determination software uses the scaled Barycentric Celestial Reference System [8] with Barycentric Dynamical Time (TDB) as coordinate time and with axes aligned with the International Celestial Reference System (ICRF) for dynamic and observation modelling. The trajectory of the

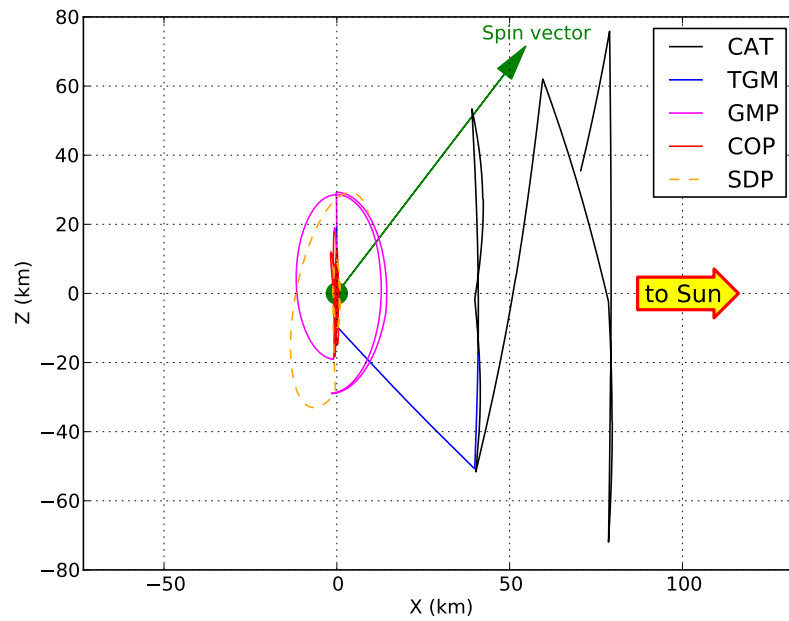
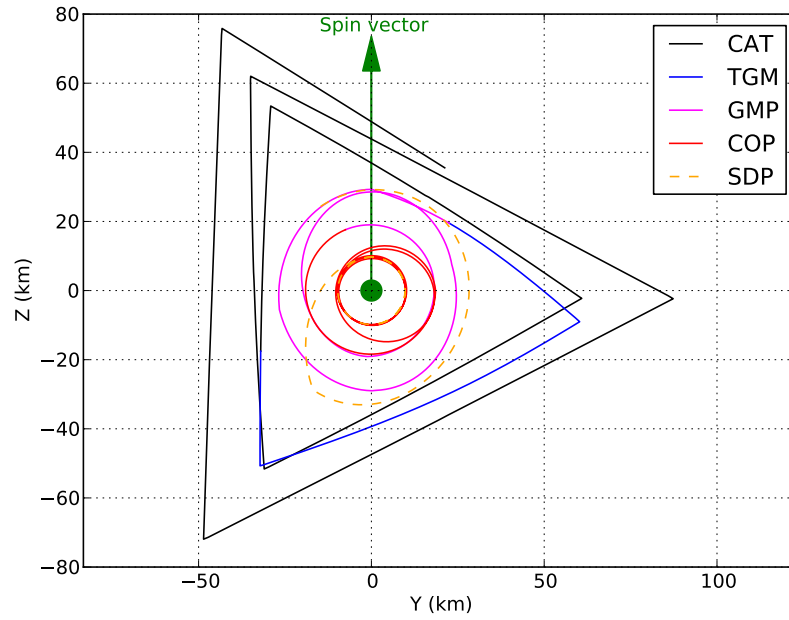


Figure 5. Orbit projection in frame defined by terminator and spin vector

comet is integrated relative to the Sun whereas the trajectory of the spacecraft is integrated with respect to the comet. In the following, we denote by \mathcal{C} our celestial reference frame with axes aligned to the ICRF axes and centred on the comet centre of mass and by \mathfrak{B} a body fixed frame. Coordinates of surface features, possible landing sites and gravity field coefficients are given in frame \mathfrak{B} . Defining this body frame was an important task of navigation which had to be done as early as possible.

2. Dynamics

2.1. Trajectory propagation

Rosetta orbit determination software numerically integrates the orbit and attitude of the comet in addition to the orbit of the spacecraft. Although the orbit and attitude dynamics of the comet are in principle coupled, it is assumed that the attitude motion is independent of the orbit so that the trajectories are generated in sequence: first the comet attitude $\mathbf{x}_1(t, \mathbf{p})$, then the comet orbit $\mathbf{x}_2(t, \mathbf{p})$ and finally the spacecraft orbit $\mathbf{x}_3(t, \mathbf{p})$, where t is TDB, the independent variable and \mathbf{p} is the vector of parameters to be estimated or considered. This sequential integration makes it possible to use different epochs for the comet attitude, comet orbit and spacecraft orbit initial states. These initial states are among the list of parameters to be estimated.

Equation 1 for $i = 1, 2, 3$ where the dot denotes time derivative has to be integrated with its associated variational equation (Eq. 2).

$$\dot{\mathbf{x}}_i = \mathbf{f}_i(\mathbf{x}_i, \mathbf{p}, t) \quad (1)$$

$$\frac{d}{dt} \left(\frac{\partial \mathbf{x}_i}{\partial \mathbf{p}} \right) = \frac{\partial \mathbf{f}_i}{\partial \mathbf{p}} + \frac{\partial \mathbf{f}_i}{\partial \mathbf{x}_i} \frac{\partial \mathbf{x}_i}{\partial \mathbf{p}} \quad (2)$$

Because of the dependencies between the different trajectories (Eq. 3 and 4), the variational equations for a trajectory are built from the solution of the variational equations for the previously generated trajectories (Eq. 5 and 6).

$$\mathbf{f}_2(\mathbf{x}_2, \mathbf{p}, t) = \tilde{\mathbf{f}}_2(\mathbf{x}_2, \mathbf{x}_1, \mathbf{p}, t) \quad (3)$$

$$\mathbf{f}_3(\mathbf{x}_3, \mathbf{p}, t) = \tilde{\mathbf{f}}_3(\mathbf{x}_3, \mathbf{x}_2, \mathbf{x}_1, \mathbf{p}, t) \quad (4)$$

$$\frac{\partial \mathbf{f}_2}{\partial \mathbf{p}} = \frac{\partial \tilde{\mathbf{f}}_2}{\partial \mathbf{p}} + \frac{\partial \tilde{\mathbf{f}}_2}{\partial \mathbf{x}_1} \frac{\partial \mathbf{x}_1}{\partial \mathbf{p}} \quad (5)$$

$$\frac{\partial \mathbf{f}_3}{\partial \mathbf{p}} = \frac{\partial \tilde{\mathbf{f}}_3}{\partial \mathbf{p}} + \frac{\partial \tilde{\mathbf{f}}_3}{\partial \mathbf{x}_2} \frac{\partial \mathbf{x}_2}{\partial \mathbf{p}} + \frac{\partial \tilde{\mathbf{f}}_3}{\partial \mathbf{x}_1} \frac{\partial \mathbf{x}_1}{\partial \mathbf{p}} \quad (6)$$

Analytical formulae of partial derivatives for all dynamic models f_1 , f_2 and f_3 are implemented in the software.

2.2. Comet attitude dynamics

The comet attitude state is the compound of the attitude quaternion q of the body frame \mathfrak{B} with respect to our celestial reference \mathfrak{C} and the angular velocity vector w in frame \mathfrak{B} (Eq. 7). The convention adopted for the quaternion is that the real part is the last component.

$$\mathbf{x}_1 = \begin{pmatrix} \mathbf{q} \\ \mathbf{w} \end{pmatrix} \quad (7)$$

Equation 8 is the compound of the attitude kinematics equation and Euler's equation of rigid body dynamics, where \mathbf{I} is the inertia tensor per unit mass in frame \mathfrak{B} , \mathbf{T} is the torque per unit mass in frame \mathfrak{B} , \otimes denotes the quaternion multiplication. This equation assumes that the centre of frame \mathfrak{B} coincides with the comet centre of mass.

$$\dot{\mathbf{x}}_1 = \begin{pmatrix} \dot{\mathbf{q}} \\ \dot{\mathbf{w}} \end{pmatrix} = \begin{pmatrix} \frac{1}{2}\mathbf{q} \otimes [\boldsymbol{\omega}, 0] \\ \mathbf{I}^{-1}(\mathbf{T} - \boldsymbol{\omega} \times \mathbf{I}\boldsymbol{\omega}) \end{pmatrix} \quad (8)$$

The parameters which can be solved or considered are the 7 components of the initial state, the 6 independent components of the symmetric matrix \mathbf{I} and the parameters of the torque models.

The torque on a comet is mainly due to its activity and is difficult to model especially when the comet shape is not known. The software has two types of basic building blocks for torque models: constant in body frame or constant in inertial frame both limited to a given time interval. In both cases the parameters to be estimated are the 3 components of the torque in a frame which is a fixed rotation from either frame \mathfrak{B} (body fixed case) or frame \mathfrak{C} (inertially fixed case). Many of these building blocks can be combined to define the total torque T .

Note that the inertia tensor and torque can only be determined up to a scale factor from the dynamics.

2.3. Comet orbit dynamics

\mathbf{x}_2 is the position and velocity vector of the comet with respect to the Centre of Integration (COI). The comet orbit dynamics is given by \mathbf{f}_2 , the difference between the comet acceleration and the COI acceleration. The COI is usually the Sun, but it can also be the Solar System Barycentre (SSB) in which case the COI acceleration is zero.

The comet as well as the COI orbits are mainly driven by gravity. \mathbf{f}_2 models the gravity due to the Sun, all 8 planets, Pluto and Earth's Moon, all as point masses from the JPL DE405 ephemeris with relativistic corrective terms for the Sun.

Additionally \mathbf{f}_2 includes a term for the non-gravitational acceleration of the comet due to its activity. This term is based on the asymmetric empirical model described in [9] but without exponential decay with time. The model has 3 parameters which size the acceleration in 3 orthogonal directions and an additional delay parameter. This empirical model was developed to support Earth-based orbit determination of comets over large time spans covering many pericentres and may not be suitable for radio tracking of a spacecraft in orbit around a comet. Our implementation of this model allows using (and solving for) different values of the 3 scale parameters for different time intervals.

2.4. Spacecraft orbit dynamics

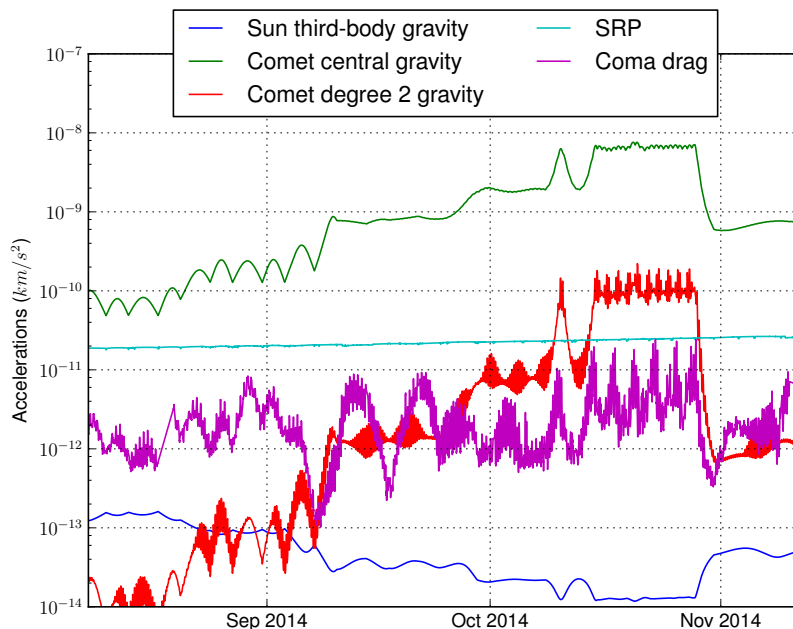


Figure 6. Spacecraft cometocentric accelerations

\mathbf{x}_3 is the position and velocity vector (\mathbf{r}, \mathbf{v}) of the spacecraft with respect to the Centre of Integration (COI). The spacecraft orbit dynamics is given by \mathbf{f}_3 the difference between the spacecraft acceleration and the COI acceleration. For Rosetta comet phase the COI is the comet. The barycentric acceleration of the COI is computed as in \mathbf{f}_2 and includes a non-gravitational term. The level of relative acceleration for different contributions during the time interval relevant for this paper is shown in Fig. 6. The non-gravitational acceleration of the COI has been omitted as it is very small during this period when the comet is still far from the Sun.

2.4.1. Gravity

The software models the gravitational acceleration due to the the Sun, all 8 planets, Pluto and Earth's Moon, all as point masses from the JPL DE405 ephemeris with relativistic corrective terms

for the Sun and the gravitational acceleration due to the the comet from Eq. 9 [10, section 3.2.4].

$$\mathbf{a}_{\text{comet gravity}} = \nabla \left[\frac{\mu}{\|\mathbf{r}\|} \sum_{n=1}^N \sum_{m=0}^{\min(M,n)} \frac{R^n}{\|\mathbf{r}\|^n} P_{nm}(\sin(\phi(\mathbf{r}))) \{C_{nm} \cos(m\lambda(\mathbf{r})) + S_{nm} \sin(m\lambda(\mathbf{r}))\} \right] \quad (9)$$

In Eq. 9, P_{nm} is the Legendre polynomial of degree n and order m , R is a reference scaling radius, μ is the comet mass parameter, C_{nm} and S_{nm} are the spherical harmonics coefficients, $\lambda(\mathbf{r})$ and $\phi(\mathbf{r})$ are respectively the longitude and latitude in frame \mathfrak{B} of the spacecraft at relative position \mathbf{r} , N and M are respectively the series truncation degree and order.

Because we choose our comet centre to be its centre of mass, we have $C_{10} = S_{10} = C_{11} = 0$. Additionally the coefficients of degree 2 can be fully determined from the inertia tensor per unit mass (Eq. 10).

$$\begin{aligned} C_{20} &= \frac{J_{xx} + J_{yy} - 2J_{zz}}{2R^2} \\ C_{21} &= \frac{-J_{xz}}{R^2} & S_{21} &= \frac{-J_{yz}}{R^2} \\ C_{22} &= \frac{J_{yy} - J_{xx}}{4R^2} & S_{22} &= \frac{-J_{xy}}{2R^2} \end{aligned} \quad (10)$$

The orbit determination program has an option to solve for the comet inertia tensor from both spacecraft orbit dynamics (via gravity) and comet attitude dynamics by expressing the degree 2 coefficients as a function of the inertias. With this option, it may be possible to resolve the indeterminacy in the scale of the inertia tensor.

2.4.2. Solar Radiation Pressure

Solar radiation pressure acceleration for Rosetta is computed a priori for a predefined spacecraft attitude, configuration and orbit and scaled in the orbit determination program. The program can be configured to use different scale factors for different time intervals and different directions. Usually we are only interested in scaling the component in the Sun direction.

2.4.3. Coma drag

The drag model is given by Eq. 11 where m is the spacecraft mass, N is the number of species in the comet atmosphere, $\rho_i(\mathbf{r})$ and $\mathbf{V}_i(\mathbf{r})$ are the density and velocity of species i at spacecraft position \mathbf{r} , \mathbf{v} is the spacecraft velocity, C_D is a coefficient set to 2, $A_i(\mathbf{r}, \mathbf{v})$ is the spacecraft effective area in direction of the relative velocity $(\mathbf{V}_i(\mathbf{r}) - \mathbf{v})$ for species i .

$$\mathbf{a}_{\text{drag}} = \frac{C_D}{2m} \sum_{n=1}^N \rho_i(\mathbf{r}) A_i(\mathbf{r}, \mathbf{v}) \|\mathbf{V}_i(\mathbf{r}) - \mathbf{v}\| (\mathbf{V}_i(\mathbf{r}) - \mathbf{v}) \quad (11)$$

The orbit determination can apply (and solve-for) scale factors (per user defined time interval) to the

drag acceleration. The effective area is computed taking into account the solar panels and a box for the spacecraft bus and neglects shadowing. Alternatively a more complex drag model that computes the drag force on each spacecraft surface (including the High Gain Antenna and the lander) taking into account shadowing is provided by our colleagues in the AOCS team [11], but this model is slower and does not provide partial derivatives with respect to the state parameters \mathbf{r} and \mathbf{v} requiring them to be computed by finite differences and is thus seldom used directly in the orbit determination program.

The atmosphere parameters (number of species with their densities and velocities) at a given point and time are provided by the operational coma software [11]. This piece of software models the densities and velocities as a function of positional parameters and time. Densities are computed as linear combination of spherical harmonics function whose coefficients may be Fourier series of time. The spherical harmonics may be defined in several frames and combined together allowing to create easily dependencies on both solar phase angle (in Sun-comet corotating frame) and latitude (in body-fixed frame). The parameters for this model are fitted from observational data such as the measurements of static pressure by the ROSINA (an instrument on board Rosetta) nude gauge or (in the case of gas velocities) come from theoretical models.

ROSINA nude gauge measurements [12] [11] are also used to produce an acceleration time series for a predetermined spacecraft attitude, configuration and orbit using the more complex model mentioned above. This time series can be used as a replacement for the drag model. However, it has gaps when the ROSINA instrument is off and it does not of course cover the future and hence, can't be used for prediction.

2.4.4. Orbit control and desaturation manoeuvres

During the phase of the mission we are interested in, manoeuvres have small delta-V and short duration and are modelled as impulsive. The orbit determination software allows to scale manoeuvres in magnitude or along 3 orthogonal axes and estimate a time delay in manoeuvre execution. Nominally we calibrate the manoeuvres using 3 scale factors along the axes of the spacecraft body frame and do not use the time offset capability. One exception is when two manoeuvres occur in a very short time interval without any observations in between (the so-called two legs manoeuvre which has to be implemented for safety reason [7]). In that case we would nominally use only one set of 3 scale factors for both manoeuvres.

3. Observable modelling

Radiometric observations are modelled as described in [13]. Ground-based optical astrometric observations as well as spacecraft based remote astrometric observations of the comet are barely used in this phase of the mission so they will not be described here. The most important observation type for relative navigation is the optical landmark observation whose model will be described in this section.

3.0.5. Body optical frame

Landmark coordinates are defined in a body optical frame, which is a scaled and translated version of the body frame \mathfrak{B} . The translation vector and scale factor can be solved by the orbit determination system. These parameters allow the usage of a set of landmark coordinates which would have been derived from stereophotogrammetry without using dynamic models in the fit. Such a set of coordinates would probably have the centre offset from the true centre of mass and the scale wrong.

3.0.6. Landmark observation model

The landmark observations are directions in camera frame of a recognisable (by a human or computer) feature on the surface of the comet. They are generated by our optical navigation group [14] from camera images using either a manual point and click method or a more autonomous correlation process between true and simulated rectified images. The observation is given as a pair $(x/z, y/z)$ where (x, y, z) are coordinates of the landmark in camera frame with X and Y directions being aligned to the CCD matrix rows and columns and the Z direction the bore-sight of the camera. They are already corrected for camera distortion effects. Since it is only used for proximity operations, the landmark observation model assumes the observation is purely geometric and does not model the light-time. However, a planetary aberration terms corrects for the combined movement of the spacecraft and comet (the aberration term is computed for the comet-centre, not for the landmark). Equation 12 is the landmark observation model.

$$\begin{pmatrix} x \\ y \\ z \end{pmatrix} = \mathbf{M}_{\text{cam}/\mathfrak{C}} \left[-\mathbf{r} + \mathbf{M}_{\mathfrak{B}/\mathfrak{C}} (\mathbf{u}\alpha + \mathbf{b}) + \frac{\|\mathbf{r}\|}{c} \mathbf{v} \right] \quad (12)$$

where \mathbf{b} and α are respectively the translation and scale between frame \mathfrak{B} and the body optical frame, \mathbf{u} is the vector of landmark coordinates in body optical frame, $\mathbf{M}_{\mathfrak{B}/\mathfrak{C}}$ is the attitude matrix of frame \mathfrak{B} with respect to frame \mathfrak{C} , $\mathbf{M}_{\text{cam}/\mathfrak{C}}$ is the attitude matrix of the camera frame with respect to frame \mathfrak{C} , \mathbf{r} and \mathbf{v} are the spacecraft position and velocity vectors in frame \mathfrak{C} and c is the speed of light.

3.0.7. Camera image bias

The inertial attitude of the camera $\mathbf{M}_{\text{cam}/\mathfrak{C}}$ is provided for each image. However, this attitude is based on gyro-stellar estimation using a predetermined alignment matrix between navigation camera and star tracker since it is not possible to see the star background in comet images. However the alignment between the different spacecraft instruments evolves due to effects such as thermal elasticity of materials. Hence it may be required to correct for mis-alignment of the camera. The orbit determination program allows to solve for 3 alignment parameters per user-defined group of cameras and per user-defined time intervals. Starting with x , y and z from Eq. 12, the final landmark

observation model is given by Eq. 13.

$$\begin{pmatrix} obs_{x/z} \\ obs_{y/z} \end{pmatrix} \begin{pmatrix} \cos(\theta_3) & -\sin(\theta_3) \\ \sin(\theta_3) & \cos(\theta_3) \end{pmatrix} \begin{pmatrix} x/z \\ y/z \end{pmatrix} + \begin{pmatrix} \theta_1 \\ \theta_2 \end{pmatrix} \quad (13)$$

where θ_1 , θ_2 and θ_3 are the image bias parameters. The observations do not allow to improve significantly the knowledge on the absolute camera attitude and thus these biases are mainly treated as consider parameters for the camera which has the most observations. However, when observations come from at least 2 cameras, the biases for the other cameras can be treated as solve-for.

4. Orbit Determination Filter

4.1. Estimation

The estimation filter used for Rosetta orbit determination is a Square Root Information Filter (SRIF)[15]. After the full trajectories and corresponding transition matrices have been built, observations equations are generated and then normalised (in case of vector observations such as landmarks they are decorrelated as part of the normalisation process). Finally the equations are sequentially added to the square root information array using Householder transforms. This process is iterated until convergence is achieved.

To facilitate convergence in the presence of strong non-linearities (this happens for example if the comet initial attitude state is rather far off from the true state), a set of equations can optionally be added to the square root information array so that it returns the solution to the damped least square problem (Levenberg-Marquart algorithm [16]).

4.2. A priori information

The solution can be constrained by optionally providing a priori values and a covariance matrix for the full set of parameters. This option is almost always used as it ensures that the linear system can be inverted (provided the a priori covariance matrix is symmetric definite). The a priori values used to constrain the parameters need not be the same as the initial values used for linearisation of the dynamic and observation models.

4.3. Treatment of comet attitude parameters

The estimator does not estimate directly the components of the comet attitude quaternion at epoch but a vector Δ of dimension 3 which is used to update the quaternion after each iteration. The update equation is Eq. 14

$$\mathbf{q}^{(i+1)} = \cos(\|\Delta^{(i)}\|)\mathbf{q}^{(i)} + \frac{\sin(\|\Delta^{(i)}\|)}{\|\Delta^{(i)}\|} \mathbf{S}(\mathbf{q}^{(i)})\Delta^{(i)} \quad (14)$$

where $\mathbf{q}^{(i)}$ is the quaternion at the beginning of iteration i , $\Delta^{(i)}$ is the solution for the Δ parameter

vector in iteration i and $\mathbf{S}(\mathbf{q})$ is a 4 by 3 matrix whose columns form an orthonormal basis of the tangent hyperplane to the unit quaternion hypersphere locally at quaternion q . This update equation ensures the norm constraint on the quaternion.

After the update of the quaternion, Δ is reset to zero and the a priori constraints equations are modified to pull the Δ vector towards the value which would bring the quaternion back towards the a priori quaternion.

A possible choice for matrix $\mathbf{S}(\mathbf{q})$ is given in Eq. 15.

$$\mathbf{S}(\mathbf{q}) = \begin{pmatrix} -q_4 & q_3 & -q_2 \\ -q_3 & -q_4 & q_1 \\ q_2 & -q_1 & -q_4 \\ q_1 & q_2 & q_3 \end{pmatrix} \quad (15)$$

For small rotations, this choice (the convention for the quaternion is that the real part is last) would lead to the components of the Δ vector being half rotation angles around the canonical axes of frame \mathfrak{B} . Another choice (Eq. 16) would allow interpreting them as half rotation angles around the canonical axes of frame \mathfrak{C} .

$$\mathbf{S}(\mathbf{q}) = \begin{pmatrix} q_4 & q_3 & -q_2 \\ -q_3 & q_4 & q_1 \\ q_2 & -q_1 & q_4 \\ -q_1 & -q_2 & -q_3 \end{pmatrix} \quad (16)$$

5. Operational setup and results

5.1. Operation schedule

During the period of the mission in which we are interested, the spacecraft commands are generated by intervals called VSTP (Very Short Term Planning). There are usually 2 VSTPs per week covering Tuesday to Friday and Friday to Tuesday. Orbit Control Manoeuvres (OCM) usually happen Wednesday and Sunday mornings. The routine orbit determination and trajectory optimization for the Tuesday to Friday planning is performed on Monday morning while for the Friday to Tuesday planning it is performed on Thursday morning. This schedule applies to most VSTPs except for a few special cases such as the VSTPs during lander delivery phase which were more frequent.

Additionally orbit determinations are run regularly to update the orbit prediction for the purpose of facilitating the optical navigation process of generating landmark observations from optical images.

The routine orbit determination uses the most recent optical observations available (i.e. from the previous night). The observation arc is usually short covering one to two weeks and in the estimation process little freedom is given to the comet dynamical and physical parameters. The update to the

comet parameters is mainly provided by off-line orbit determination using observations spanning a large time interval (up to several months). We call this process a long arc orbit determination, while the routine orbit determination used for planning or updating predictions is referred to as short arc orbit determination.

5.2. Body frame definition, attitude and gravity field determination

In early August 2014, our colleagues in the optical navigation group had provided us with an estimate for the comet spin period and pole direction [17], [14]. There was no visible evolution in the period and spin axis direction with time. The obvious choice for the body frame was then to take the Z axis along the spin direction. We achieved this uniform rotation motion around body Z in the orbit determination by constraining the angular velocity to the body Z direction, giving freedom in the attitude quaternion around X and Y, setting the inertia tensor to the identity matrix (since it could not be resolved from the attitude dynamics) and not using torques. Using the first set of landmark observations, the first estimate for the mass parameter of the comet was derived. We had hoped beforehand that the comet would be subjected to a small torque-free nutation motion which would have helped us determine the inertia matrix and centre of mass accurately. The principal axes of inertia would have then defined a natural body frame. As more observations came in, we tried with increasingly longer arcs, solving for the inertia matrix (one diagonal term was fixed since the dynamics is left unchanged by scaling the tensor) and initial angular velocity for a given arbitrary attitude quaternion at epoch without obtaining any meaningful results: any free nutation motion had to be within the noise. The scaled inertia matrix would have given us the 5 degree 2 terms of the gravity field to one scale factor. With the uniform rotation, we knew that the pole Z was the principal axis of highest inertia and that C_{21} and S_{21} must be zero. That left us with determining 3 coefficients C_{20} , C_{22} and S_{22} instead of one scale factor.

Approximate principal axes of inertia for the comet were determined using a preliminary shape model under the uniform mass distribution assumption. And the X or prime-meridian direction was originally chosen as the projection of the computed principal axis of lowest inertia on the XY plane towards the smaller lobe of the comet. It is to be noted that apart from the uniform mass distribution assumption, this inertia tensor computation contains significant errors due to the shape model being incorrect in the then unobserved region of the comet (southern latitudes). The coordinates of the landmarks were then rotated to this frame.

Lacking knowledge on the comet inertias, the prime meridian had to be defined relative to surface features rather than dynamically. Had we used a single landmark to define the prime meridian, it would have been difficult to guarantee the observability of the prime meridian during any orbit determination arc. Instead, it was chosen that many landmarks would participate in the definition of the prime meridian in the sense that there should be no average rotation around the Z axis between two sets of landmark coordinates solutions. Moreover it cannot be guaranteed in the long term that defining Z as the spin vector direction will always be valid since it could happen in the future that the spin vector starts moving noticeably and significantly relative to the averaged surface features. Therefore the frame definition is now embedded in an evolving subset of the best estimated landmarks.

Worse, the absence of nutation meant that the position of the centre of mass along the Z direction could not be resolved by the comet attitude motion but only weakly determined by the gravitational pull on the spacecraft. This initially led to a correlated uncertainty in the Z coordinates of all landmarks larger than 100 meters and an increased uncertainty in the estimated comet mass. The initial variability of the landmark Z coordinates between the different solutions was problematic and it was decided to fix the estimated centre of mass positions between different orbit determinations until we reached closer orbits when the determination accuracy would improve significantly. This was because the frame was used to communicate between the scientists, the lander team and the Rosetta Mission Operations Centre, in particular to specify coordinates of landing sites. This required a stable definition of the body frame.

A rough estimate for the comet mass was obtained in early August but it was not until October, one month to landing, when Rosetta was orbiting at 20 kilometres distance and below, that reliable estimates for the mass distribution in the form of gravitational spherical harmonics coefficients of degree and order 2 then 3 were derived. The last mass distribution update, including a 7 meters shift in the centre of mass position along the Z axis, was performed in early November, less than 2 weeks to landing.

It also became apparent, a few weeks before landing, that the spin period of about 12.4 hours was not so constant and thus that the comet was subjected to a torque. The increase in rotation period of then only about one second per month was modelled as a constant torque from September 10 onwards and aligned with the Z axis of $-1.2 \times 10^{-15} \text{ rad.s}^{-2}$. Since our inertia tensor is set to unity, we actually use angular rate rate which is more intuitive (the actual torque is not known precisely, because the moment of inertia around Z is not known). The evolution of the torque could not be predicted and thus it was not possible to make accurate long term prediction (over several months) of the comet rotational state.

5.3. Coma drag modelling

The drag acceleration is almost fully radial and in first approximation via the coma density should follow an inverse square law with the cometocentric distance. Gravity has the same properties. Additionally the density likely depends on longitude and latitude of the sub-satellite point. So does gravity. However the density may also depend on the distance, longitude and latitude of the Sun and is of a stochastic nature, with a possibly high time variability. Moreover the acceleration due to drag depends linearly on the cross-sectional area that the spacecraft is showing towards the comet, which, in turn, depends mainly on solar phase angle via the solar panel. During the CAT phase, because the spacecraft is showing a large cross-sectional area towards the comet and the range of phase angle flown is very limited, it is difficult to accurately determine the comet mass since part of it may be absorbed in the drag scale factor.

Thanks to the ROSINA instrument, we have a measure of the evolution of the density along the trajectory. Assuming gas velocity from theoretical models, we can determine an acceleration profile for the spacecraft that the orbit determination just has to scale. Short gaps in ROSINA data are filled using the operational coma model. The positional parameters of interest in setting up the operational model are mainly the latitude and solar phase angle (Fig. 4). This is because the latitude

and solar phase angle vary slowly while the longitude cycles in half a day. In off-line analysis, the coefficients for the model are fitted to match recent ROSINA data [11].

During each VSTP preparation, an orbit determination is first performed using the operational coma model alone to obtain a scale factor. Then a second orbit determination is performed using the ROSINA derived acceleration profile (and the coma model for the gaps but with the scale for the coma model fixed). Finally the scaled drag acceleration profiles for both runs are compared. If the profiles do not match at all, but could be made to match significantly better by splitting the arc into a 2 or 3 meaningful subintervals (such as terminator, day side, south latitude...) for which different scale factors for the coma model are estimated, then the separation of the scale factor into these subintervals is performed and the process restarted. The scale factor obtained in the last subinterval is also used for prediction.

5.4. Information content and weighting of observations

Landmark observations provide a direct measurement of the relative state. They are very sensitive to changes in longitude and latitude but not so much to changes in the distance to the comet. The measurement accuracy in longitude and latitude is approximately the camera pixel angular size: for the NAVCAM, this corresponds to about 10 meters at 100 km, 1 meter at 10 km. However, changing the distance to the comet by 200 meters at a distance of 100 km would only change the size of the comet in the image by one pixel.

Doppler and range observations provide information on the comet geocentric distance and, thanks to the Earth rotation, also on right ascension and declination of the comet [18]. Because of the low absolute equatorial declination of the target (less than 15 degrees during the period of interest), the information on declination obtained from radio-tracking is poor resulting in a large uncertainty in the comet cross-track components of position and velocity.

While the long term signal in Doppler and range data is useful to determine the comet orbit, the short term signal gives precise line of sight information for the relative orbit. The landmark observations alone do not provide immediate information and accurate time resolution for changes in relative velocity. For the line of sight direction, this information is better provided by short term signatures in the Doppler observations. In particular Doppler data is very useful to calibrate manoeuvres.

Short arc orbit determination always use landmark and Doppler observations. If the comet orbit is fixed from a previous long arc solution, range data is not used as it would probably be heavily biased for the newly acquired data. If the used long arc orbit solution for the comet orbit is a bit too old (e.g. more than a week), the Doppler observations cannot usually be fitted well. In that case, the comet orbital state is solved-for with an a priori constraint obtained from mapping a previous long arc solution and the range data is then used in the fit.

Two-way coherent Doppler and range measurements in X band are provided almost around the clock during this critical phase by the ESTRACK 35 meters Deep Space Antennas at New Norcia, Malargüe and Cebreros as well as by the 34 to 70 meters antennas of the JPL/DSN complexes at Goldstone, Madrid and Canberra. 2-way range observations are weighted at 5 meters and 2-way

Doppler observations with a 300 seconds count time are weighted at 0.1 millimetre per second. The Root Mean Square of the post-fit residuals for typical orbit determinations is about 0.6 meter for range and 0.04 millimetre per second for Doppler.

Landmarks observations are assigned a covariance matrix (in practice always diagonal) during their creation. Their inverse weight is in average slightly above one pixel. Before including them in the orbit determination, they are de-weighted by a factor of 2 (covariance matrix multiplied by 4). The resulting inverse weights vary from 0.3 to 13 pixels with an average of 2.7 pixels (13.5 millidegrees). The Root Mean Square of the post-fit residuals for typical orbit determinations is about one pixel (5 millidegrees). The normalized post-fit statistics are about 0.1 for range and 0.5 for Doppler and landmark observations.

5.5. Filter configuration

5.5.1. Long arc orbit determination

Tables 2 and 3 summarize the filter setup for a long arc orbit determination covering September 3 to October 28 including 4951 range observations, 10662 Doppler observations from 6 ground stations and 28387 observations of 986 landmarks from 2 cameras. The post-fit residuals for this orbit determination are shown in Fig. 7 and Fig. 8. The epoch is set to October 15.

In total there are 3737 solve-for parameters and 79 consider parameters of which 530 are dynamic parameters.

The quality of the orbit determination is evaluated from the residual plots and statistics as well as from the estimates and post-fit variances of the parameters. It is in particular interesting to look at the estimates for the range biases (Fig. 9) and desaturation manoeuvres (Fig. 10) as these parameters can easily absorb some modelling errors.

Figure 11 shows the consider post-fit formal 3σ errors for the relative state mapped over the whole observation arc. Black dashed vertical lines correspond to orbit control manoeuvre times. The formal uncertainties for the comet heliocentric trajectory are much larger: 3 km and 0.3 mm/s radial, 15 km and 0.4 mm/s along-track, up to 90 km and 1 cm/s cross-track (all 3σ).

In this setup, the comet attitude is constrained by enforcing that body Z is along the pole and not allowing rotation of the quaternion around body Z (although after many iterations a small rotation around body Z between initial and final quaternion may occur via a sequence of small rotations around X and Y) and landmarks are free. In some other long arc setups freedom is given to rotate around body Z but landmark positions and an a priori covariance matrix for the full set of landmark coordinates (from a previous non-overlapping solution) is input to constrain the attitude quaternion.

The new coordinates of the landmark are compared to the best set of previously determined landmark coordinates and are rotated around body Z by a small angle that minimizes the drift of the prime meridian in body frame. Simultaneously, the comet attitude trajectory (and in principle gravity field coefficients) are rotated with that same angle.

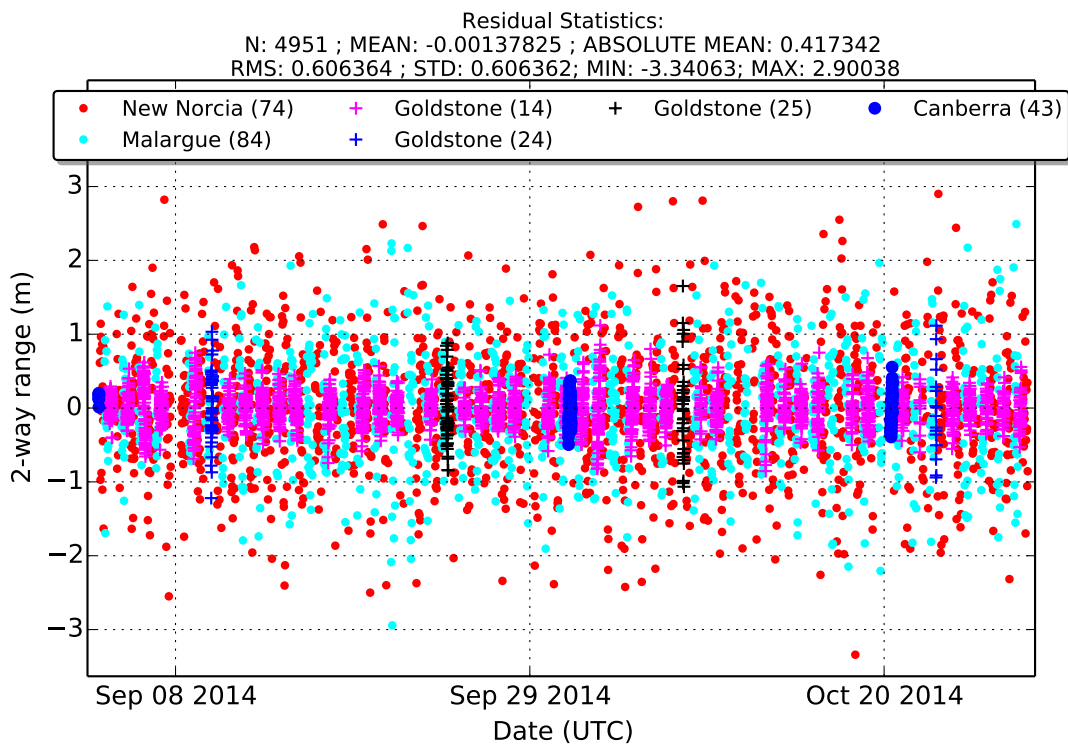
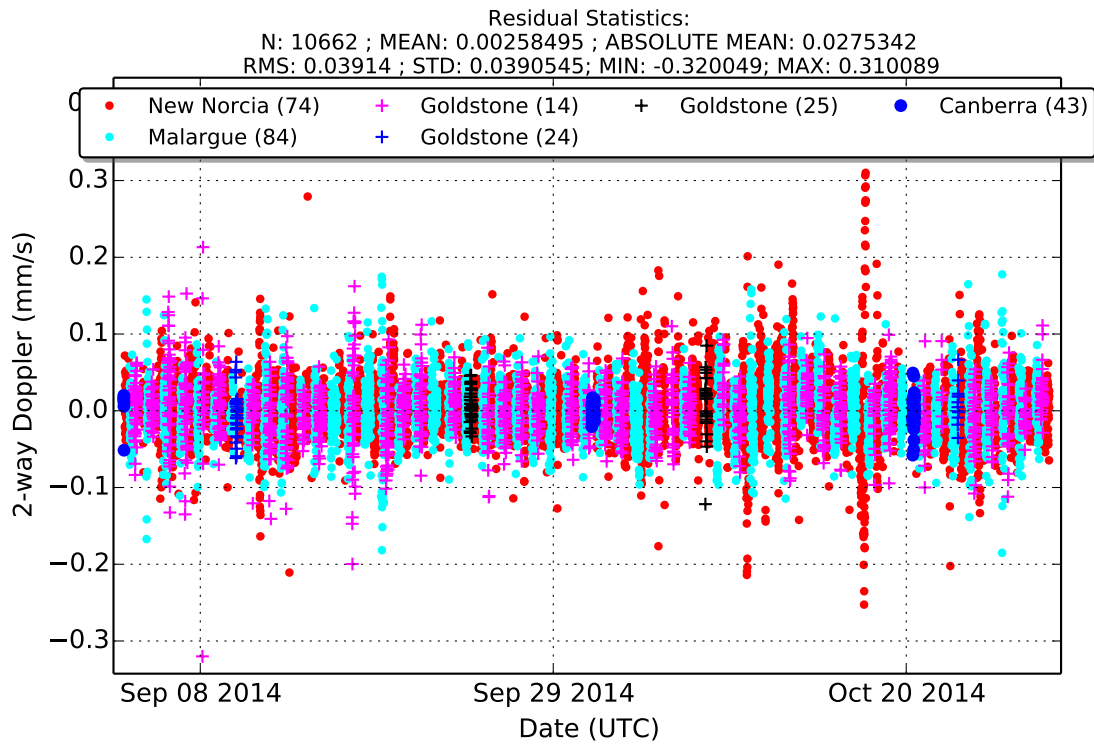


Figure 7. Doppler and Range post-fit residuals

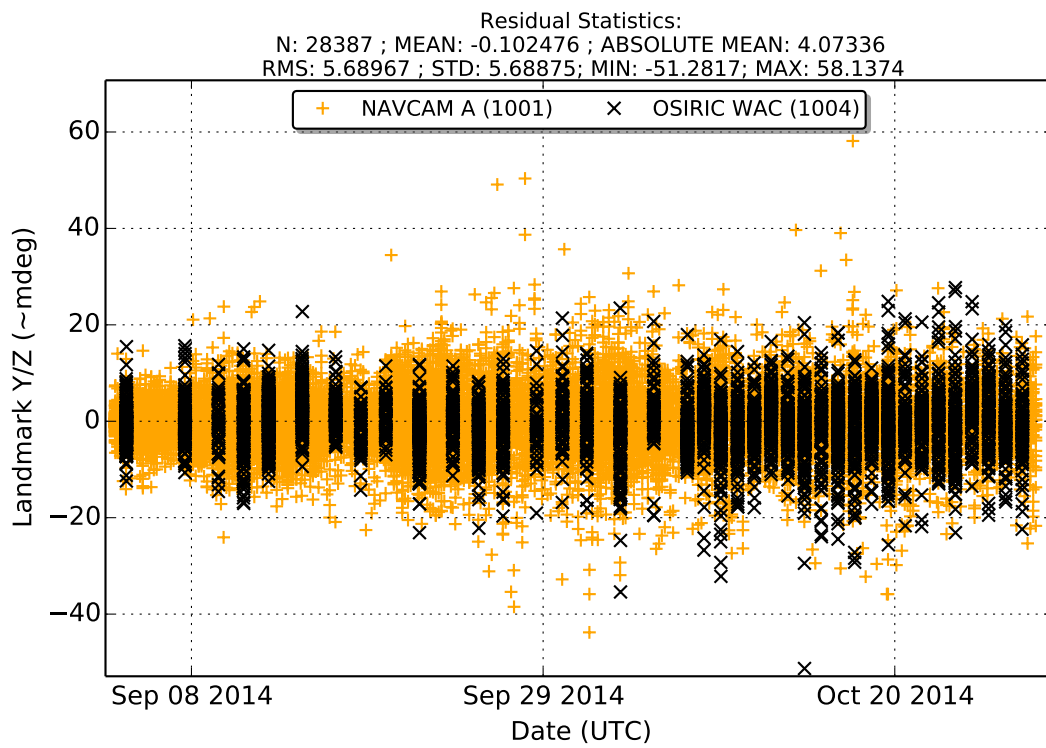
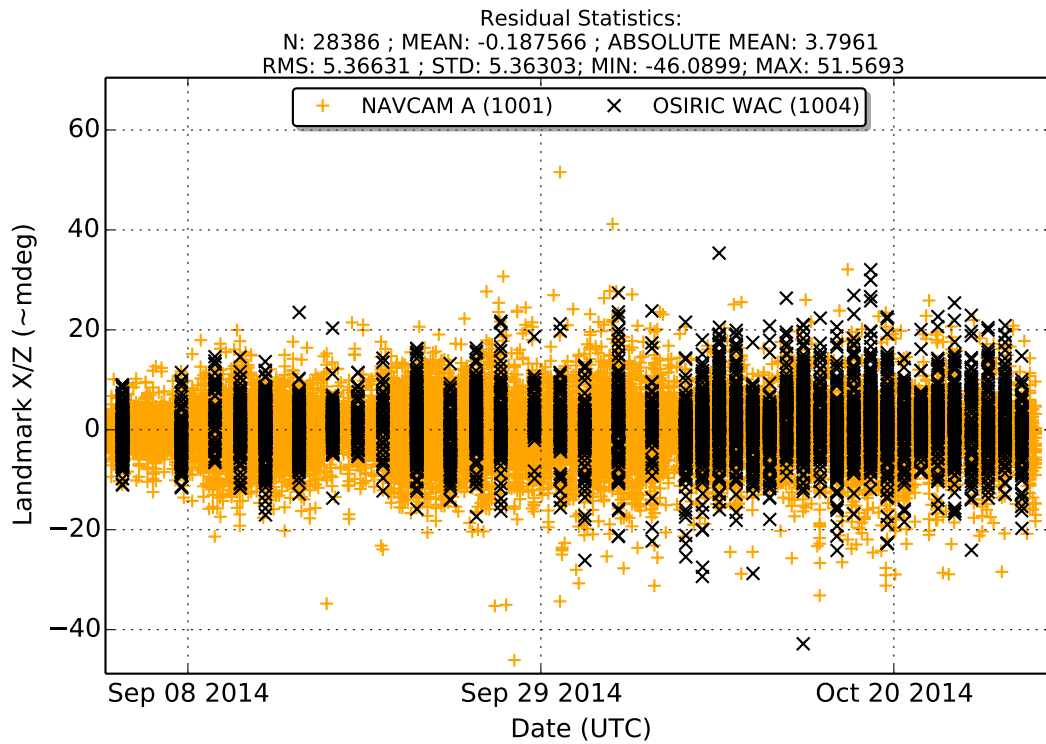


Figure 8. Landmarks post-fit residuals

Table 2. Example long arc filter setup (Dynamic parameters)

Parameter	Type	A priori value and constraint
Spacecraft relative state at epoch	solve-for	virtually unconstrained, values from latest orbit determination
Comet heliocentric state at epoch	solve-for	constrained, mapped from previous non-overlapping long-arc orbit determination
Comet attitude state at epoch (quaternion)	solve-for around body X and Y, fixed around body Z	from latest orbit determination virtually unconstrained around X and Y
Comet attitude state at epoch (angular rates in body frame)	X and Y components fixed, Z solved-for	X and Y rates set to zero, Z rate from latest orbit determination with $\sigma = 7\%$
Comet non-gravitational acceleration parameters	consider	from ultra-long ground-based comet orbit determination
Comet angular rate around Z from September 10 onwards	solve-for	a priori set to zero, $\sigma = 1 \times 10^{-14} rad.s^{-2}$
SRP scale factors	solve-for in radial direction, consider in orthogonal directions	last value determined during cruise, $\sigma = 3\%$ in radial direction and $\sigma = 0.05\%$ of total SRP acceleration in orthogonal directions
comet GM	solve-for	value from previous long arc orbit determination, virtually unconstrained
spherical harmonics coefficient 4x4 (with reference radius = 1 km)	solve-for except C10, C11, S11, C21, S21 fixed to zero	values set to zero a priori except for degree 2 terms set from previous long arc, $\sigma = 1.0$
drag acceleration scale factor using operational coma model	solve-for	global bias $\sigma = 100\%$ plus exponentially correlated stochastic process in 12 hours intervals with autocorrelation time 3 days and steady state $\sigma = 100\%$
Desaturation manoeuvres in spacecraft frame	solve-for	zero a priori $\sigma = 0.333mm/s$ for each direction
Trajectory Control Manoeuvres in spacecraft frame	solve-for	values from previous orbit determinations, constrained to about 3% in magnitude and 1.7 degree in direction (one σ)

Table 3. Example long arc filter setup (Measurement parameters)

Parameter	Type	A priori value and constraint
Landmark coordinates in body frame	solve-for	values from previous solutions or zero, virtually unconstrained
Camera alignment per camera	consider	$\sigma = 10mdeg$ per axis
Pole position error	consider	$\sigma = 30nrad$ for both X and Y
UT1 error (Earth rotation)	consider	$\sigma = 750\mu s$
Transponder group delay error	consider	$\sigma = 10ns$
Wet tropospheric delay calibration error per station complex	consider	$\sigma = 4cm$
Dry tropospheric delay calibration error per station complex	consider	$\sigma = 1cm$
Ionospheric delay calibration error per station complex	consider	$\sigma = 25\%$
One-way range biases per pass	solve-for	$\sigma = 5m$
ESTRACK ground stations position errors	consider	$\sigma = 10cm$ per axis and per station
DSN ground stations position errors	consider	full covariance matrix provided by JPL

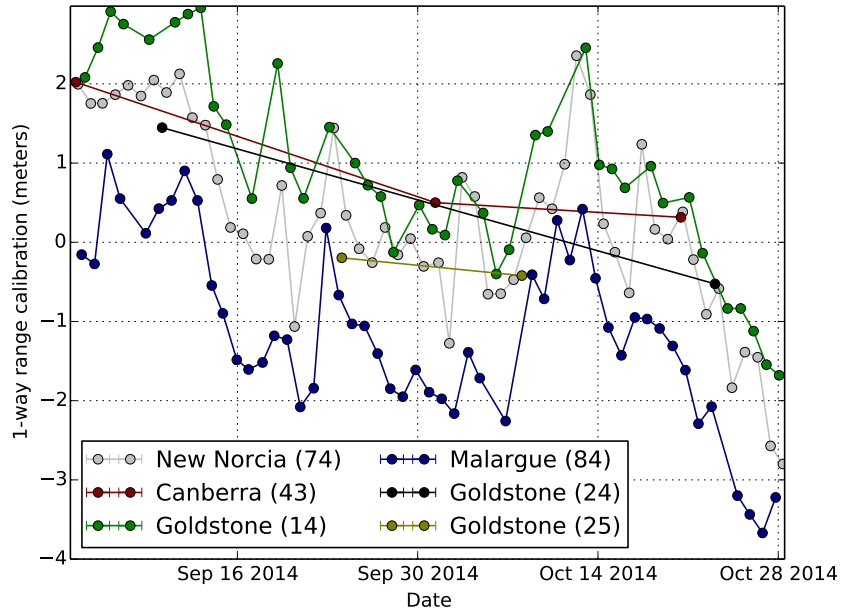


Figure 9. Range biases estimates

This long arc used the operational coma model for the drag with one scale factor every 12 hours. Since the drag is the most uncertain dynamic model, it is important to give enough degrees of freedom and try different configurations to evaluate how mis-modelling of the drag could affect other parameters such as centre of mass position (landmark coordinates especially along body Z) and gravity field coefficients. This configuration was re-run with the ROSINA acceleration profile with one scale factor for the whole arc (plus another scale factor for all the ROSINA data gaps together using the operational coma model). This led to very similar results for the centre of mass and the 3 by 3 gravity field.

5.5.2. Short arc

The routine short arc orbit determination is mainly concerned with relative orbit prediction. Comet dynamic and physical parameters are either fixed or very constrained from a long arc solution. Landmark coordinates are fixed for well determined landmarks, solved-for for the others. Pole direction, angular rate and rate rate are fixed or considered while some freedom is given to rotate the attitude quaternion at epoch around body Z.

5.6. Reconstruction and prediction accuracy

Due to modelling errors, the reconstruction accuracy cannot be assessed directly from the formal covariance matrix resulting from the orbit determination process. However the consistency between solutions using different configuration and especially the direct measure of the errors in the longitude and latitude provided by the landmarks make it possible to see that the reconstruction accuracy is a few meters in the bound orbits between 10 and 30 kilometres radius which is close to the formal

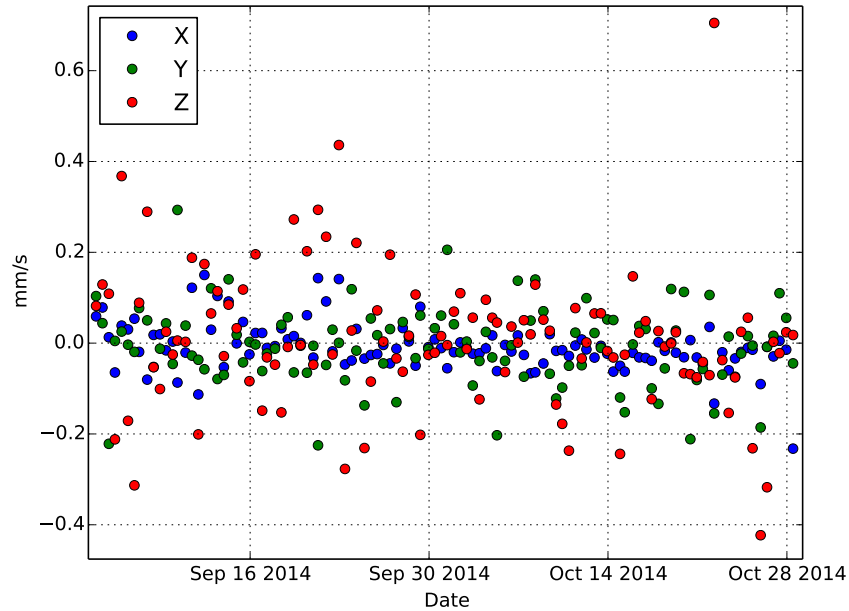


Figure 10. Desaturation manoeuvre estimates in spacecraft frame

uncertainties shown in Fig. 11.

Figure 12 shows the prediction errors assuming reconstruction errors are negligible. In the upper plot, red dashed vertical lines correspond to orbit control manoeuvre times. The switch between greyed area and white area corresponds to VSTP boundaries. The pointing error is computed for the centre of the comet. As expected, the prediction errors often get worse towards the end of each VSTP. The cross-track errors are usually small while along-track errors are the largest followed by radial errors. The along-track (and cross-track) errors lead to pointing errors in the camera images which have to be minimized for science purpose but also for navigation. When the comet gets out of the field of view of the NAVCAM, images cannot be used for navigation. It was important that by the mornings of each VSTP planning days (usually Monday and Thursday), the comet was still in the field of view of the NAVCAM (pointing error less than 2.5 degrees). Otherwise, the orbit would have had to be raised.

As expected largest pointing errors occur in the lower orbits and especially when going down in an elliptical orbit. Comparing the pointing errors in the GMP phase and in the SDP phase both at a radius of 30 kilometres shows a significant improvement in prediction. This is the result of the accurate determination of the comet physical parameters: centre of mass and gravity field.

The prediction accuracy is limited by the stochastic errors in the OCM and desaturation manoeuvres. Orbit determination results for OCM calibration is shown in Tab. 4. Manoeuvres with SLOT in their name correspond to stochastic manoeuvres that may not be required: 3 of them were skipped.

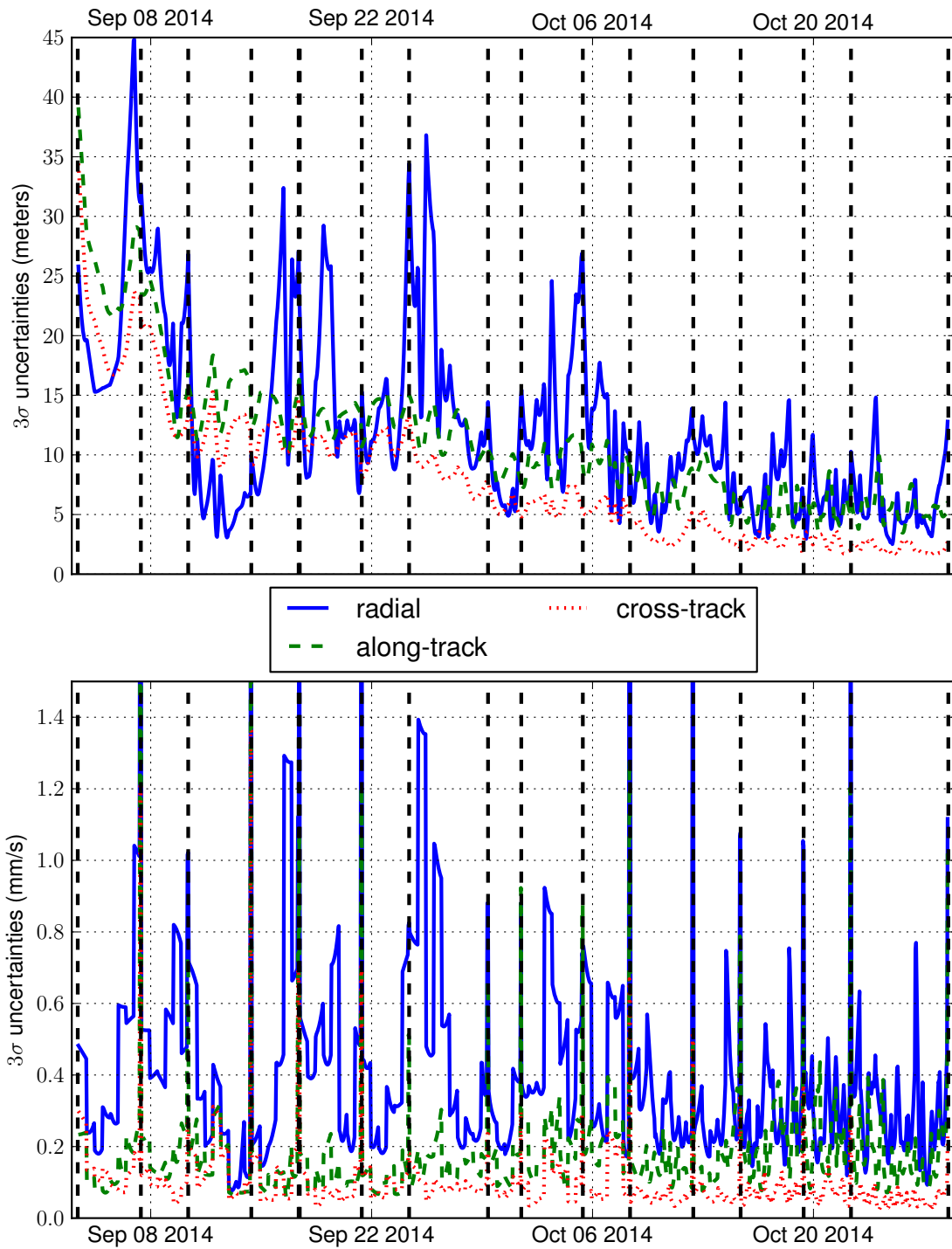


Figure 11. Formal state covariance evolution for reconstructed relative orbit

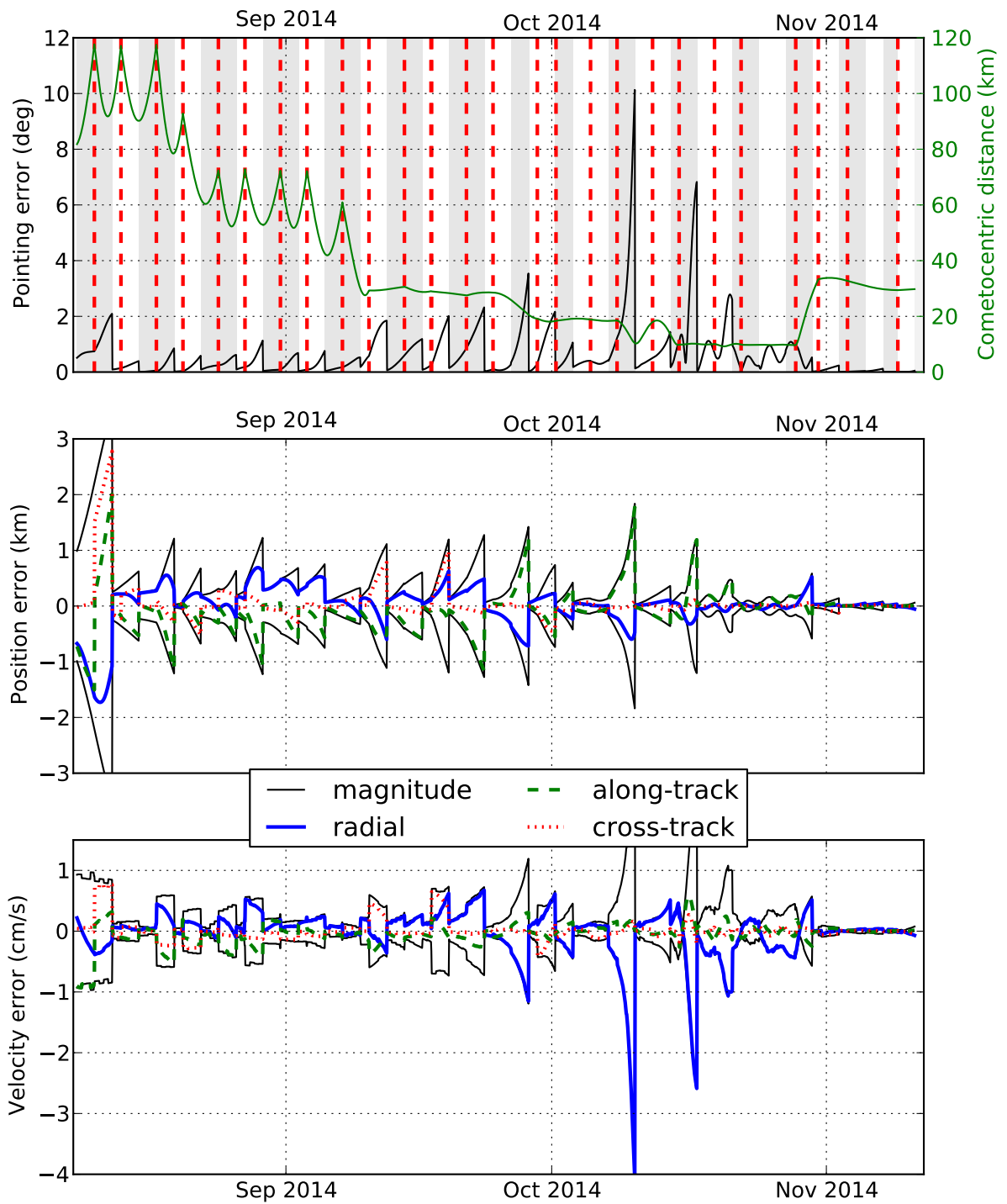


Figure 12. Orbit prediction error shown as predicted minus reconstructed

Table 4. OCM calibration

Manoeuvre	Date	ΔV (mm/s)	Performance calibration (%)
CAT-INSERTION	2014-08-06	892	+0.4
CAT-CHANGE-1	2014-08-10	882	-0.2
CAT-CHANGE-2	2014-08-13	871	-0.3
CAT-CHANGE-3	2014-08-17	857	+0.1
CAT-CHANGE-4	2014-08-20	738	+0.04
CAT-CHANGE-5	2014-08-24	604	+0.1
CAT-CHANGE-6	2014-08-27	589	+0.02
CAT-CHANGE-7	2014-08-31	593	-0.3
TGM-1	2014-09-03	565	-0.1
TGM-2	2014-09-07	452	-0.3
GMP-1	2014-09-10	193	-2.4
GMP-SLOT-1	2014-09-14	25	-6.5
GMP-2 (2 legs)	2014-09-17	85 and 88	-4.0
GMP-SLOT-2	2014-09-21	19	-6.6
GMP-3	2014-09-24	16	-7.6
GMP-4	2014-09-29	106	-3.2
GMP-SLOT-2.5	2014-10-01	14	-6.2
GMP-SLOT-3	2014-10-05	10	-6.5
COP-1	2014-10-08	37	-4.3
COP-SLOT-1	2014-10-12	22	-4.8
COP-2	2014-10-15	57	-4.9
COP-SLOT-2	2014-10-19	12	-4.7
COP-SLOT-3	2014-10-22	12	-2.6
SDP-SLOT-1	2014-10-25	not needed	
SDP-1	2014-10-28	82	-2.7
SDP-2	2014-10-31	96	-2.4
SDP-SLOT-2	2014-11-03	5	-7.4
SDP-SLOT-7-DAY	2014-11-05	not needed	
SDP-SLOT-3-DAY	2014-11-09	3	-2.4
SDP-SLOT-1-DAY	2014-11-11	not needed	

5.7. Comet physical parameters

Table 5 lists the values and formal uncertainties of the comet dynamical and physical parameters that were used for the SDP phase. They were estimated in a long arc orbit determination very similar to the one described in section 5.5.1. (same observation arc, slightly different configuration). The gravity field coefficients are given for a reference radius of 1 km. The uncertainty in the pole direction is mainly due to the uncertainties in the cameras alignment.

Table 5. Comet dynamical and physical parameters

Parameter	Value	Consider sigma
Rotation axis right-ascension [deg]	69.42	0.01
Rotation axis declination [deg]	63.988	0.005
Rotational period at 2014/10/15 [s]	44655.96	0.01
Torque around Z (from September 10 onwards) [10^{-15} rad/s^2]	-1.21	0.03
GM [$10^{-7} \text{ km}^3/\text{s}^2$]	6.665	0.002
C20:	-5.54×10^{-1}	2.4×10^{-3}
C22:	2.03×10^{-1}	1.9×10^{-3}
S22:	-8.18×10^{-3}	1.2×10^{-3}
C30:	-3.8×10^{-1}	2.3×10^{-2}
C31:	-1.42×10^{-1}	8.9×10^{-3}
S31:	1.1×10^{-1}	1.7×10^{-2}
C32:	6.1×10^{-2}	7.7×10^{-3}
S32:	-2.7×10^{-2}	5.7×10^{-3}
C33:	8×10^{-3}	3.0×10^{-3}
S33:	-5.0×10^{-2}	3.2×10^{-3}

It is to be noted that the gravity field coefficients are close to the ones computed under uniform density assumption from recent shape models (July 2015) that cover the whole comet, even though no shape models were used in deriving them.

6. Conclusion and outlook

The characterisation of the comet performed mainly in the three months from arrival to lander delivery has allowed Rosetta to navigate safely and accurately around the comet and Philae to touch down hundred meters from the targeted landing point, well within the mission requirements. The errors in determining the heliocentric orbit are large but the comet-relative orbit can be determined quite well. The main source of modelling errors in the dynamics was the drag due to the coma, while the most problematic source of errors in the measurements was the camera mis-alignment. Orbit prediction accuracy is also limited by the desaturation manoeuvres and the mis-performance of the OCMs. The determination of the centre of mass and gravity field to degrees and order 3, performed in the close orbits, has significantly improved the navigation accuracy.

After Philae landing, the comet has presented new challenges to the orbit determination process: larger non-gravitational accelerations and torques, causing also an evolution in the spin axis. This has made it difficult to fit the comet orbit and attitude over long time spans. Moreover, long arc

orbit determination required to understand the evolution of the comet parameters does not converge easily: work is in progress on a multi-arc (or multiple shooting) orbit determination with arc boundaries matching constraints to provide a continuous trajectory solution (currently published comet trajectories present large discontinuities). Also, some landmarks have disappeared or moved due to remodelling of surface features by comet activity around perihelion (August 2015) which is problematic, since our body frame is defined by the landmark coordinates. The navigation requirements are currently reduced because Rosetta is kept very distant from the comet, but a new comet characterisation phase will be needed for the operations at low altitude in 2016.

7. Acknowledgement

Drawings were produced with LibreOffice Draw using images from openclipart.org and ESA, plots were generated with matplotlib and this paper was compiled with pdflatex.

8. References

- [1] T. Morley, F. Budnik. “Rosetta Navigation at its First Earth Swing-by.” “Proceedings of the 19th International Symposium on Space Flight Dynamics, Kanazawa,” 2006.
- [2] F. Budnik, T. Morley. “Rosetta Navigation at its Mars Swing-by.” “Proceedings of the 20th International Symposium on Space Flight Dynamics, Annapolis,” 2007.
- [3] T. Morley, F. Budnik. “Rosetta Navigation for the Fly-by of Asteroid 2867 Steins.” “Proceedings of the 21st International Symposium on Space Flight Dynamics, Toulouse,” 2009.
- [4] T. Morley, F. Budnik, M. Croon, B. Godard. “Rosetta Navigation for the Fly-by of Asteroid (21) Lutetia.” “Proceedings of the 25th International Symposium on Space Flight Dynamics, Pasadena,” 2012.
- [5] T. Morley, F. Budnik, B. Godard, P. Muñoz, V. Janarthanan. “Rosetta navigation from reactivation until arrival at comet 67P/Churyumov-Gerasimenko.” “Proceedings of the 25th International Symposium on Space Flight Dynamics, Munich,” 2015.
- [6] P. Muñoz, F. Budnik, V. Companys, B. Godard, C. Casas, T. Morley, V. Janarthanan. “Rosetta navigation during lander delivery phase and reconstruction of Philae descent trajectory and rebound.” “Proceedings of the 25th International Symposium on Space Flight Dynamics, Munich,” 2015.
- [7] P. Muñoz, F. Budnik, B. Godard, T. Morley, V. Companys, U. Herfort, C. Casas. “Preparations and strategy for navigation during Rosetta comet phase.” “Proceedings of the 25th International Symposium on Space Flight Dynamics, Pasadena,” 2012.
- [8] B. Godard, F. Budnik, T. Morley, A. Lopez Lozano. “Relativistic acceleration of planetary orbiters.” “Proceedings of the 23rd International Symposium on Space Flight Dynamics, Pasadena,” 2012. Also available online: http://issfd.org/ISSFD_2012/ISSFD23_OD1_5.pdf.

- [9] D.K. Yeomans, P.W. Chodas. “An asymmetric outgassing model for cometary nongravitational accelerations.” *Astronomical Journal* 98, 1989. Also available online: <http://articles.adsabs.harvard.edu/full/1989AJ.....98.1083Y/0001083.000.html>.
- [10] O. Montenbruck, E. Gill. *Satellite Orbits*. Springer, 2000.
- [11] C. Bielsa, Michael Müller, U. Herfort. “Operational approach for the modeling of the coma drag force on Rosetta.” “Proceedings of the 24th International Symposium on Space Flight Dynamics, Pasadena,” 2014. Also available online: http://issfd.org/ISSFD_2014/ISSFD24_Paper_S11-2_Bielsa.pdf.
- [12] C. Bielsa, M. Müller, G. Huguet. “Prediction of the coma drag force on Rosetta.” “Proceedings of the 23rd International Symposium on Space Flight Dynamics, Pasadena,” 2012. Also available online: http://issfd.org/ISSFD_2012/ISSFD23_OD2_6.pdf.
- [13] T.D. Moyer. “Formulation for Observed and Computed Values of Deep Space Network (DSN) Data Types.” Tech. rep., Jet Propulsion Laboratory (JPL), 2000. http://descanso.jpl.nasa.gov/Monograph/series2/Descanso2_all.pdf.
- [14] R. Pardo de Santayana, M. Lauer. “Optical Measurements for Rosetta navigation near the comet.” “Proceedings of the 25th International Symposium on Space Flight Dynamics, Munich,” 2015.
- [15] G.J. Bierman. *Factorization Methods for Discrete Sequential Estimation*. Academic Press Inc., New York, 1977.
- [16] “Wikipedia entry on Levenberg-Marquart algorithm.” https://en.wikipedia.org/wiki/Levenberg%E2%80%93Marquardt_algorithm.
- [17] F. Castellini, D. Antal-Wokes, R. Pardo de Santayana, K. Vantournhout. “Far Approach Optical Navigation and Comet Photometry for the Rosetta Mission.” “Proceedings of the 25th International Symposium on Space Flight Dynamics, Munich,” 2015.
- [18] C.L. Thornton, J.S. Border. *Radiometric Tracking Techniques for Deep-Space Navigation*. JPL, 2000. Also available online: http://descanso.jpl.nasa.gov/monograph/series1/Descanso1_all.pdf.
- [19] U. Herfort, C. Casas. “Trajectory preparation for the approach of spacecraft Rosetta to comet 67P/Churyumov-Gerasimenko.” “Proceedings of the 25th International Symposium on Space Flight Dynamics, Munich,” 2015.